INFRARED Fe II EMISSION IN NARROW-LINE SEYFERT 1 GALAXIES

A. RODRÍGUEZ-ARDILA[1] AND S. M. VIEGAS

Instituto Astronômico e Geofísico, Universidade de São Paulo, Av. Miguel Stefano 4200, CEP 04301-904, São Paulo, SP, Brazil

M. G. PASTORIZA

Departamento de Astronomia, UFRGS. Av. Bento Gonçalves 9500, CEP 91501-970, Porto Alegre, RS, Brazil

AND

L. PRATO[1]

Department of Physics and Astronomy, University of California, Los Angeles, CA 90095-1562

Received 2001 April 26; accepted 2001 September 26

ABSTRACT

We obtained 0.8–2.4 μm spectra at a resolution of 320 km s^{-1} of four narrow-line Seyfert 1 galaxies in order to study the near-infrared properties of these objects. We focus on the analysis of the Fe II emission in that region and the kinematics of the low-ionization broad lines. We show that the 1 μm Fe II lines (λ9997, λ10501, λ10863, and λ11126) are the strongest Fe II lines in the observed interval. For the first time, primary cascade lines of Fe II arising from the decay of upper levels pumped by Lyα fluorescence are resolved and identified in active galactic nuclei. Excitation mechanisms leading to the emission of the 1 μm Fe II features are discussed. A combination of Lyα fluorescence and collisional excitation is found to be the main contributor. The flux ratio between near-IR Fe II lines varies from object to object, in contrast to what is observed in the optical region. A good correlation between the 1 μm and optical Fe II emission is found. This suggests that the upper z^4F^0 and z^4D^0 levels from which the bulk of the optical Fe II lines descend are mainly populated by the transitions leading to the 1 μm lines. The width and profile shape of Fe II λ11127, Ca II λ8642, and O I λ8446 are very similar but significantly narrower than Paβ, giving strong observational support to the hypothesis that the regions where Fe II, Ca II, and O I are produced are cospatial, interrelated kinematically, and most probably located in the outermost portion of the broad-line region.

Subject headings: infrared: galaxies — galaxies: active — galaxies: Seyfert

1. INTRODUCTION

Narrow-line Seyfert 1 galaxies (hereafter NLS1s) are a peculiar group of Seyfert 1 objects, recognized by Osterbrock & Pogge (1985) for their following optical properties: (1) the broad components of the permitted lines have FWHM < 2000 km s^{-1}, narrower than those of the classical Seyfert 1 galaxies (i.e., $\sim$4000 km s^{-1}), (2) the [O III]/Hβ ratio is less than 3, and (3) usually, strong Fe II emission dominates the optical and ultraviolet spectrum. In the soft and hard X-ray bands NLS1s also seem to have peculiar properties. In most cases they are characterized by a very steep spectrum and extreme and rapid variability (Boller, Brandt, & Fink 1996; Leighly 1999). Up to now, no single model could explain all of the observed properties of these objects, and much effort has recently been made in order to understand their central engines. Variability studies (Peterson et al. 2000) point out that the ultimate cause for their peculiar behavior may be attributable to a smaller black hole mass ($\sim$10^6 $M_\odot$) together with a near- or super-Eddington accretion rate.

NLS1s are ideal objects for studying many features that are clearly separated in their spectra but are heavily blended in classical Seyfert 1 galaxies because of the broadness of their permitted lines. Such is the case with the Fe II emission lines, which produce a ubiquitous pseudocontinuum from the ultraviolet through the near-IR. This pseudocontinuum carries a large amount of energy from the broad-line region

(BLR) and is not yet well understood. In the optical and UV regions, the Fe II lines have been well studied (Wills, Netzer, & Wills 1985; Joly 1991; Lipari, Terlevich, & Macchetto 1993). The main processes believed to contribute to the bulk of that emission are continuum fluorescence via UV resonance lines, self-fluorescence via overlapping Fe II transitions, and collisional excitation. Nonetheless, most models that include these processes cannot account for the observed strength of the Fe II lines. Penston (1987), Sigut & Pradhan (1998), and Verner et al. (1999) considered that fluorescent excitation by Lyα may be important in understanding the Fe II spectrum in active galactic nuclei (AGNs) from the ultraviolet to the IR. However, the lack of suitable data in the latter region has hindered tests of predictions.

In the near-IR region, Fe II emission lines has been mostly observed in a variety of Galactic emission-line stars (Hamann & Persson 1989; Rudy et al. 1991; Hamann et al. 1994). At least in these sources, the Fe II lines redward of 7000 Å can be attributed to cascades from excited states that are pumped by resonant absorption of H I Lyα. In all cases, the strongest Fe II lines are the ones located at 9997, 10171, 10490, 10501, 10863, and 11126 Å, emitted after the decay of the common upper term (b^4G). Because of their close proximity in wavelength, they are termed the 1 μm Fe II lines. Other important Fe II lines also detected in Galactic sources are located in the 8500–9300 Å interval. They are primary cascade lines descending from the upper 5p levels to the lower e^4D and e^6D terms. With the advent of a new generation of IR detectors with greater sensitivity and resolution in this region, it is now possible to search for these lines in AGNs, mainly in NLS1s, and test the validity of the models of Fe II emission. This is a crucial step in

understanding the physical processes at work in the central engines of these objects.

The only detection to date of the 1 μm Fe II lines in an AGN was reported by Rudy et al. (2000, hereafter RMPH) in their 0.8–2.5 μm spectrophotometric observation of I Zw 1, the archetypical NLS1. Their data clearly reveal Fe II $\lambda 9997$, $\lambda 10501$, $\lambda 10863$, and $\lambda 11126$. Based on the absence of the crucial cascade lines that feed the common upper state where the 1 μm Fe II lines originate (assuming Lyα fluorescence as the dominant mechanism) as well as the relatively low energy of that state, RMPH suggest that the observed lines are collisionally excited. No individual identification of Fe II lines in the 8500–9300 Å interval has yet been done in Seyfert galaxies, but it is believed that the strong broad feature, centered at 9220 Å and observed in many AGNs, is in part due to Fe II (Morris & Ward 1989).

In this paper we present midresolution ($\sim$320 km s^{-1}), near-IR spectroscopy of four NLS1s (1H1934$-$063, Ark 564, Mrk 335, and Mrk 1044) not previously observed in this spectral region whose optical spectra reveal strong to moderate Fe II emission. In § 2 we present the observations, data reduction, and a brief description of the most conspicuous spectroscopic features observed in each galaxy. The excitation mechanism of the Fe II lines and the observed relative intensity are discussed in § 3. The kinematics of the BLR derived from the low-ionization lines is treated in § 4. Conclusions are presented in § 5.

2. OBSERVATIONS, DATA REDUCTION, AND RESULTS

2.1. Observations

The data were obtained at the NASA 3 m Infrared Telescope Facility (IRTF) on 2000 October 11 and 13 (UT) with the SPEX facility spectrometer (Rayner et al. 1998, 2002). In the short wavelength cross-dispersed mode, SPEX provides nearly continuous coverage from 8200 to 24000 Å. Ten minute integrations, nodding in an off-on-on-off source pattern, were combined to produce final spectra. Typical total integration times ranged from 30 to 40 minutes. A0V stars were observed near targets to provide telluric standards at similar air masses. Seeing was $\sim$1$\farcs$0. A 0$\farcs$8 slit yielded an instrumental resolution of 320 km s^{-1}.

2.2. Data Reduction

The spectral extraction and wavelength calibration procedures were carried out using SPEXTOOL, the in-house software developed and provided by the SPEX team for the IRTF community (Cushing, Vacca, & Rayner 2002).[2] Each on-off source pair of observations was reduced individually and the results summed to provide a final spectrum. A 1$''$ or 3$''$ (in the case of 1H1934$-$063) aperture was used to extract the spectra. Observations of an argon arc lamp enabled wavelength calibration of the data; the rms of the dispersion solution for the four target galaxies was $\sim$2 $\times$ 10^{-5} μm.

Wavelength-calibrated final target spectra were divided by AOV stars observed at a similar air masses. However, even small differences in air mass between the target galaxies and standard stars resulted in residuals, primarily evident in the spectrum of Mrk 1044. The spectra were each multiplied by a blackbody function corresponding to 10,000 K in order to restore the true continuum shape of the targets.

Spectra were flux calibrated by normalizing to the K-band magnitude, 6.303 mag, of one of the observed A0V standard stars, HD 182761. We used the task STANDARD of the ONESPEC package of IRAF[3] for this purpose. In this process, a blackbody flux distribution based on the magnitude and spectral type of the star was employed. The error in the flux calibration is $\sim$10%, estimated from comparison with an overlapping visual wavelength, red spectrum of 1H1934$-$063 at 0.8–0.95 μm and previously published IR spectrophotometry for MRK 335 (Rudy et al. 1982). Nonetheless, this calibration is not absolute. For this reason, the uncertainties quoted in this paper reflect the errors derived from the signal-to-noise ratio (S/N) of the spectra.

We correct the spectra for Galactic extinction, as determined from the *COBE/IRAS* infrared maps of Schlegel, Finkbeiner, & Davis (1998). The value of the Galactic $E(B-V)$ as well as basic information for each object are listed in Table 1. Finally, each spectrum was shifted to rest wavelength. The value of z adopted was determined by averaging the redshift measured from the strongest lines, usually O I $\lambda 8446$, [S III] $\lambda 9531$, Fe II $\lambda 9997$, Paδ, He I $\lambda 10830$, O I $\lambda 11287$, Paβ, Paα, and Brγ. In all cases, the radial velocities were in very good agreement with the values reported in the literature.

2.3. Results

The resulting extracted spectra in the 0.8–2.4 μm wavelength interval, corrected for redshift, are displayed in Figures 1–4. Identification of the known emission lines is given for each spectrum. Prominent lines of Fe II, H I, He I, O I, and Ca II are observed in the four galaxies, similar to those present in I Zw 1. In addition, He II $\lambda 10124$ as well as [S III] $\lambda 9070$, $\lambda 9531$, [S VIII] $\lambda 9912$, [S IX] $\lambda 12523$, [Fe II] $\lambda 12567$, [Si X] $\lambda 14305$, and [Si VI] $\lambda 19630$, not present in I Zw 1, are clearly detected in our data. A detailed analysis of the narrow emission lines is beyond the scope of this paper and will be discussed in a future publication (A. Rodríguez-Ardila et al. 2002a, in preparation).

In order to measure the flux of the emission lines, we have assumed that they can be represented by a single or a sum of Gaussian profiles. The LINER routine (Pogge & Owen 1993), a χ^2 minimization algorithm that fits as many as eight Gaussians to a profile, was used for this purpose. Table 2 list fluxes and FWHMs for the detected Fe II and other permitted lines. The FWHM values were corrected for instrumental broadening ($\sim$320 km s^{-1}). Except for Fe II $\lambda 10501$ and $\lambda 11127$, which are isolated features, the Fe II lines are blended with He I $\lambda 10830$ plus Paγ (Fe II $\lambda 10863$) or He II $\lambda 10124$ plus Paδ (Fe II $\lambda 9956$, $\lambda 9997$, and

---

[2] SPEXTOOL is available from the IRTF Web site at http://irtf.ifa.hawaii.edu/Facility/spex/spex.html.

[3] IRAF is distributed by NOAO, which is operated by AURA Inc., under contract to the NSF.

TABLE 1

BASIC INFORMATION OF THE NARROW-LINE SEYFERT 1 GALAXIES

Galaxy	z	M_v[a]	A_v[b]	Morphology
1H1934$-$063......	0.01059	$-$19.04	0.972	Sb
Ark 564	0.02468	$-$20.42	0.198	SB
Mrk 335	0.02578	$-$21.32	0.118	S0/a
Mrk 1044	0.01645	$-$18.84	0.113	SB0

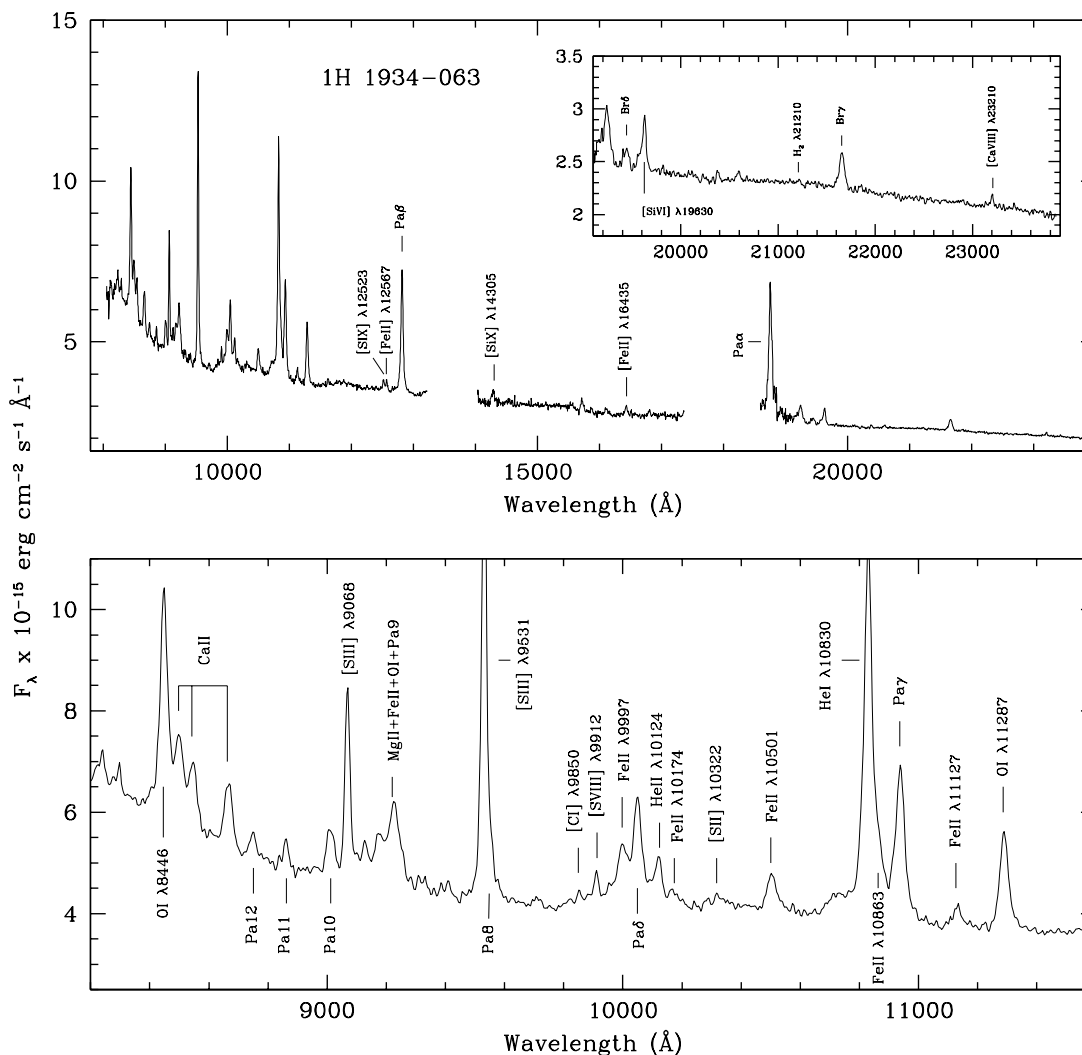[a] A value of $H_0 = 75$ km s^{-1} Mpc^{-1} was assumed.
[b] Galactic extinction.

Fig. 1.—Near-IR spectrum of the NLS1 1H1934−063 in rest wavelengths. The upper panel shows the spectrum in the wavelength interval 0.8–2.4 μm, and the box in the upper right is a zoom of the K-band spectrum, with the identification of the most important emission lines. The lower panel displays the spectrum around 1 μm and identifies the Fe II and other permitted and forbidden lines present in this region.

$\lambda10171$). For consistency, in these latter cases the Fe II and Paschen lines were constrained to have the same width as those derived for Fe II $\lambda11127$ and Paβ, respectively. Nonetheless, it is interesting to note that even if no constraint was imposed, the resulting line widths were in agreement with those found for the isolated lines.

The above procedure also allowed us to separate the contribution of the narrow-line region (NLR) in those lines that are emitted both in the BLR and the NLR. The results show that in the Paschen lines, for instance, nearly half the total flux is emitted by the NLR, very similar to what was found by Rodríguez-Ardila et al. (2000a) for the Balmer lines. Table 3 list the fluxes and FWHMs of the Paschen and He I $\lambda10839$ lines that could be deblended into a narrow and broad component. All the values of FWHM were corrected for instrumental broadening. In Mrk 1044 it was not possible to find a consistent solution for Paδ, Paγ, and He I $\lambda10839$ because of the lower S/N of the spectrum. For this reason, the total fluxes associated with each of the latter three lines are reported but must be understood as the sum of the contribution of both the NLR and BLR.

The presence of emission from the NLR is demonstrated by the observation of strong [S III] $\lambda9068$ and $\lambda9531$. In

order to test the validity of the Gaussian approximation, we used the technique applied by Rodríguez-Ardila et al. (2000a) to separate the narrow and broad flux in Paβ, which consists of using the profile of a line known to be emitted exclusively in the NLR as a template. In the current work, we assumed that the width of the narrow component of the permitted lines would be similar to that of [S III] $\lambda9531$, the strongest forbidden line observed. Based on this assumption, [S III] $\lambda9531$ was scaled to the peak intensity of a given permitted line and then subtracted off in different proportions until the residuals consist of a pure broad component with no absorption superimposed. This procedure has the advantage of being free from any assumption regarding the form of the line profiles. The results were almost identical to those obtained using the Gaussian approximation. Figure 5 shows examples of the deblending of Paβ and the region around Paδ for Ark 564.

In the rest of this section we will give brief descriptions of the most important features observed in the NLS1 spectra.

2.3.1. *1H1934−063*

1H1934−063 is a relatively poorly known NLS1 but an excellent laboratory to study many emission-line processes.
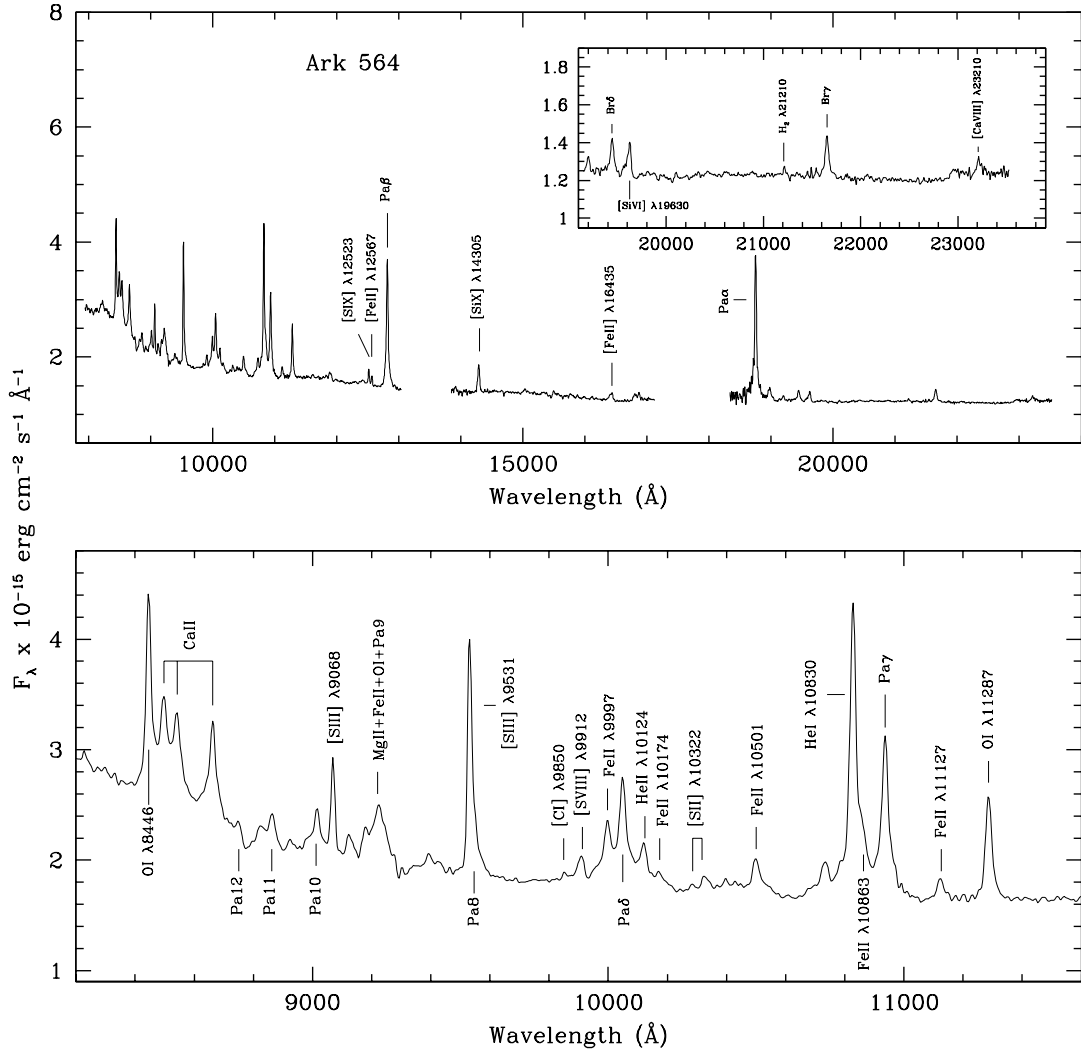
FIG. 2.—Same as Fig. 1, but for Ark 564

TABLE 2
OBSERVED EMISSION-LINE FLUXES AND FWHM FOR THE PERMITTED LINES

LINE	1H1934−063		ARK 564		MRK 335		MRK 1044	
	Flux	FWHM	Flux	FWHM	Flux	FWHM	Flux	FWHM
Fe II λ8927	...	...	0.18 ± 0.05	580	0.34 ± 0.13	700	0.22[a]	...
Fe II λ9127	2.13 ± 0.41	950	0.59 ± 0.11	600	0.72 ± 0.23	900	0.91 ± 0.29	1050
Fe II λ9177	2.77 ± 0.41	950	0.75 ± 0.15	600	1.83 ± 0.23	900	0.38 ± 0.25	1050
Fe II λ9202	1.90 ± 0.41	950	0.52 ± 0.15	600	1.38 ± 0.23	900	...	...
Pa9 λ9229	5.00 ± 0.42	950	1.91 ± 0.20	820	4.52 ± 0.31	1250	2.60 ± 0.47	1900
Fe II λ9256	0.80 ± 0.25	500	0.46 ± 0.20	800	0.66 ± 0.21	900	...	...
Fe II λ9956	1.24 ± 0.28	1000	0.54 ± 0.07	750	...	...	0.63 ± 0.07	1000
Fe II λ9997	4.52 ± 0.28	1000	1.72 ± 0.07	750	4.36 ± 0.12	1600	1.36 ± 0.07	1000
He II λ10124......	3.44 ± 0.30	1100	1.72 ± 0.13	1650	3.62 ± 0.14	1850	1.06 ± 0.14	1800
Fe II λ10171	0.85 ± 0.28	1000	0.38 ± 0.07	750	0.77 ± 0.12	1600	0.22 ± 0.07	1000
Fe II λ10501	2.62 ± 0.25	1000	1.30 ± 0.09	1100	1.83 ± 0.23	1600	1.16 ± 0.28	1620
Fe II λ10863	4.24 ± 0.25	950	0.99 ± 0.08	700	...	...	1.31 ± 0.17	900
Fe II λ11127	1.30 ± 0.23	850	0.54 ± 0.07	600	0.55 ± 0.14	1100	0.52[b]	...
O I λ11287	6.91 ± 0.24	850	2.70 ± 0.07	600	3.87 ± 0.17	1100	1.52 ± 0.17	900
Paα λ18761[b]......	25.43	970	13.46	600	20.76	1200	4.21	1200
Brγ λ21655	2.24 ± 0.14	850	1.05 ± 0.06	600	2.67 ± 0.31	1150	0.78 ± 0.91	1000

NOTE.—Fluxes are in units of 10^{-14} ergs cm^{-2} s^{-1} and FWHM in units of km s^{-1}.
[a] Upper limit.
[b] Flux measurement affected by atmospheric absorption, so it represents a lower limit.
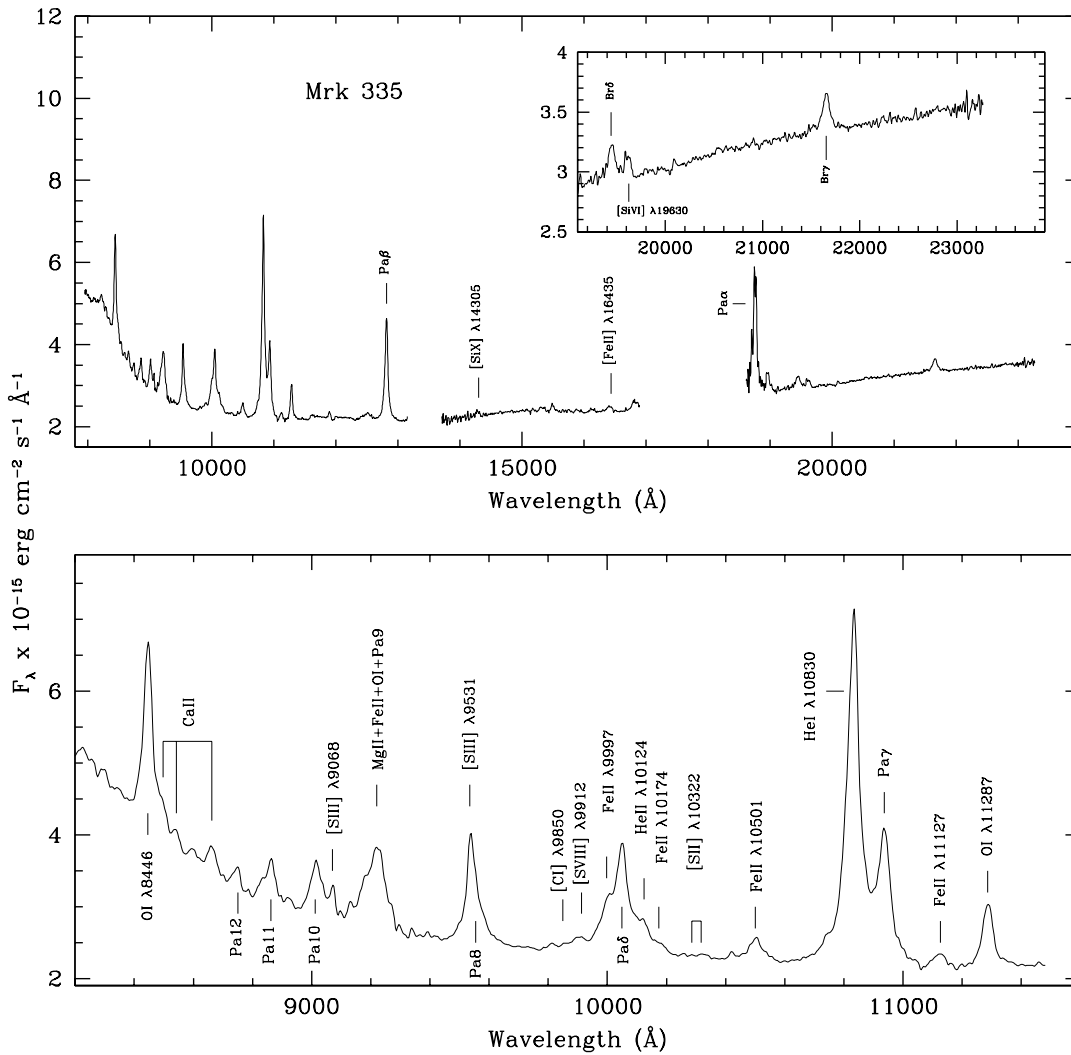
FIG. 3.—Same as Fig. 1, but for Mrk 335

Its optical spectrum, described by Rodríguez-Ardila et al. (2000a), is full of both permitted and forbidden lines. High-ionization lines such as [Fe x] and [Fe xiv] are very prominent. In the near-IR it also displays a very rich spectrum, both in permitted and forbidden lines (see Fig. 1). He i λ10830, Paα, Paβ, Paδ, O i λ8446, λ11287, the Ca ii triplet in emission, and the 1 μm Fe ii lines are strong. In addition,

Brγ and Brδ are clearly observed. A very conspicuous blend of low-ionization species, centered in 9220 Å, is present. We identified Fe ii λ9177, λ9202, and λ9256 as well as Pa9 λ9227 as contributors to this feature. Mg ii λ9218 and λ9244 are probably present but heavily blended with the Pa9. The continuum emission is very steep and follows a simple power-law form. High-ionization forbidden lines of [S viii],

TABLE 3

OBSERVED EMISSION-LINE FLUXES AND FWHM FOR THE PERMITTED LINES WITH BROAD AND NARROW COMPONENTS

LINE	1H1934−063		ARK 564		MRK 335		MRK 1044	
	Flux	FWHM	Flux	FWHM	Flux	FWHM	Flux	FWHM
Paδ_n λ10049	...	...	1.00 ± 0.03	320	...	...	...	...
Paδ_b λ10049	7.58 ± 0.27	1000	3.16 ± 0.10	1650	5.86 ± 0.09	1100	2.85 ± 0.09	1250
He i$_n$ λ10830......	7.53 ± 0.20	410	4.90 ± 0.08	370	5.49 ± 0.14	550	...	...
He i$_b$ λ10830......	19.6 ± 0.33	1230	5.46 ± 0.41	2400	24.10 ± 0.44	2020	8.35 ± 0.19	1000
Paγ_n λ10937	4.29 ± 0.25	570	1.84 ± 0.07	320	...	...	...	...
Paγ_b λ10937	9.22 ± 0.41	1600	4.00 ± 0.29	1700	11.60 ± 0.24	1500	3.92 ± 0.28	1500
Paβ_n λ12820	8.36 ± 0.22	600	3.95 ± 0.08	400	4.29 ± 0.13	600	2.22 ± 0.10	600
Paβ_b λ12820	9.64 ± 0.39	1800	5.90 ± 0.30	1800	12.73 ± 0.36	2050	3.18 ± 0.27	2300

NOTE.—Fluxes are in units of 10^{-14} ergs cm^{-2} s^{-1} and FWHM in units of km s^{-1}. The subscripts "n" and "b" stand for narrow and broad components, respectively.
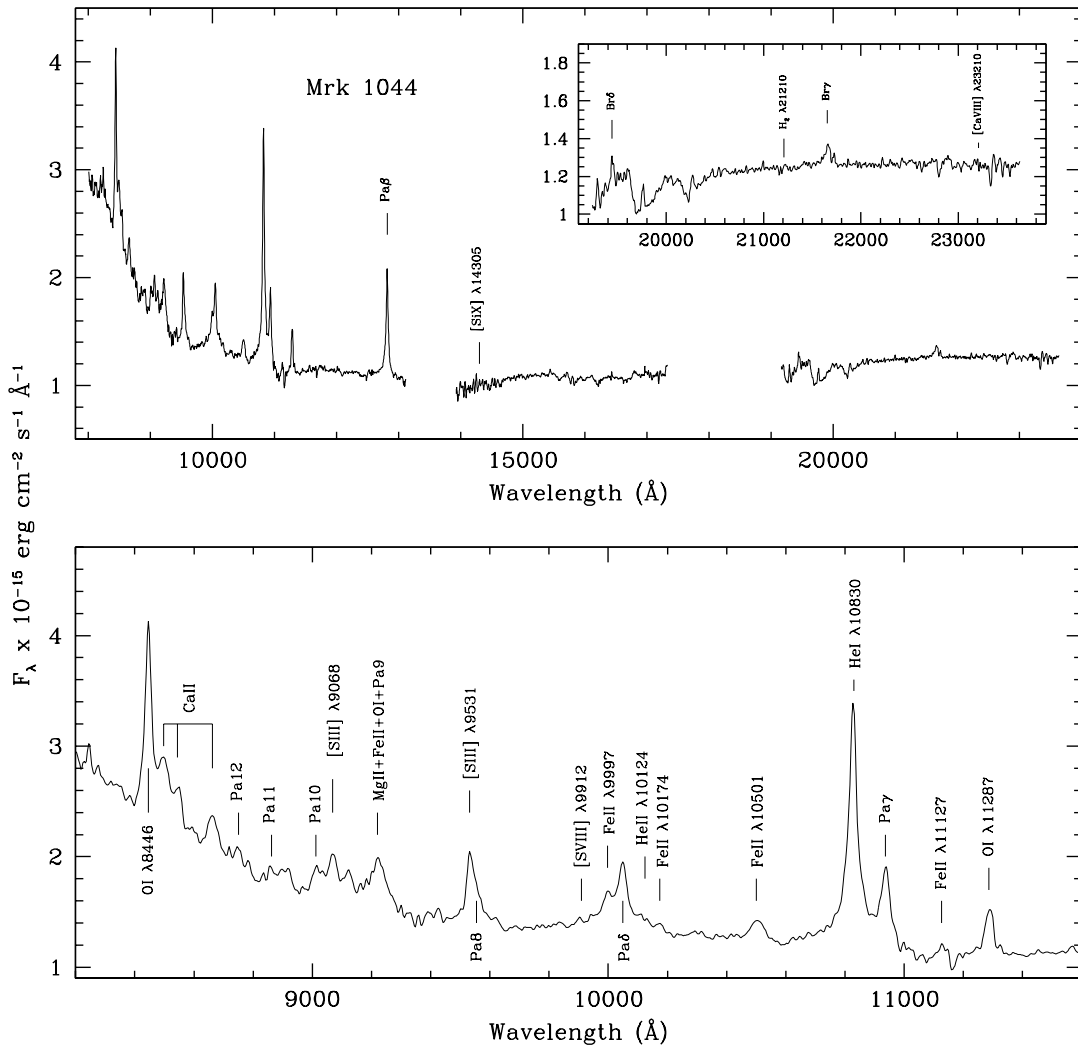
FIG. 4.—Same as Fig. 1, but for Mrk 1044

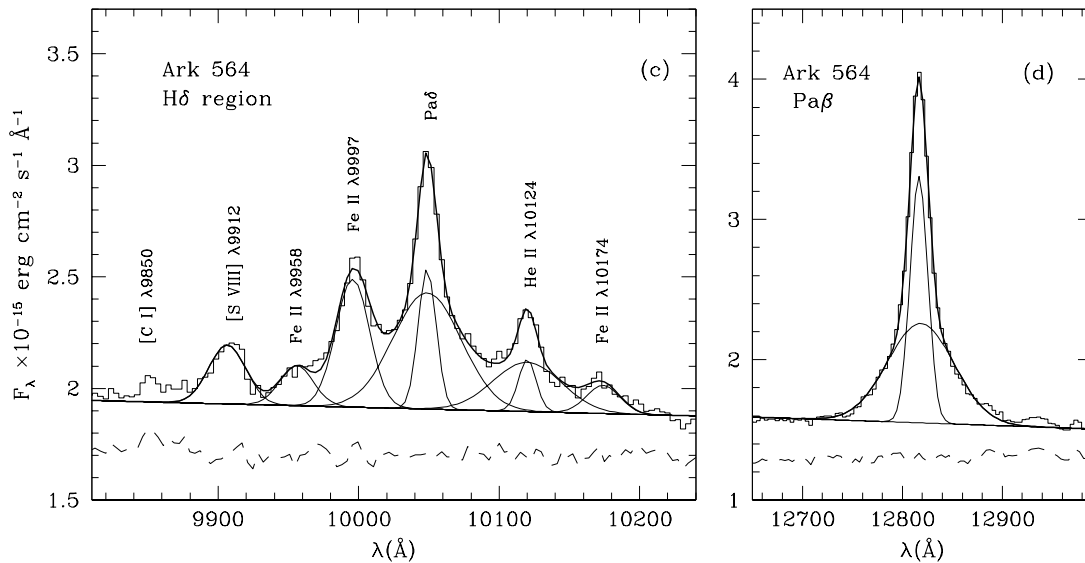FIG. 5.—Example of the deblending procedure applied to Paβ and Paδ for Ark 564. The histogram is the data and the thick line the fit to the observed blend. Individual Gaussian components are thin lines. The residuals of the fits are dashed lines.

[S IX], [Si X], [Si VII], and [Ca VIII] are clearly visible as well as a blip at the expected position of the line H_2 (1, 0)S(1) at 2.122 μm. [S III] λ9531 is, by far, the strongest forbidden line detected.

2.3.2. Ark 564

Ark 564 is a widely known and well-studied NLS1, mainly in the UV and X-ray region (Boller et al. 1996; Crenshaw et al. 1999; Comastri et al. 2001; Ballantyne, Iwasawa, & Fabian 2001). It is the brightest NLS1 in the 2–10 keV range; the *ROSAT* and *ASCA* observations reveal a complex X-ray spectrum (Vaughan et al. 1999). In the near-IR this object is also very rich in emission lines (see Fig. 2), similar in intensity to those of 1H1934−063. The permitted lines are rather narrow, just slightly broader than the forbidden lines. The 1 μm Fe II lines are strong and well resolved. Brγ is clearly detected as well as the molecular H_2 line (1, 0)S(1) at 2.121 μm. He I λ10830, the Ca II triplet, and O I $\lambda\lambda$8446, 11287 are all strong. The λ9220 blend is present with Fe II λ9177, λ9202, λ9256, Pa9, and Mg II λ9244 clearly resolved. The forbidden line spectrum is remarkable, displaying strong low- and high-ionization lines such as [S III] λ9068, 9031, [C I] λ9850, [S VIII] λ9912, [S II] λ10286, λ10322, [S IX] λ12523, [Si X] λ14305, and [Si VI] λ19630. The continuum emission rises steeply from Paβ to shorter wavelengths and is flat between 1.5 and 2.4 μm.

2.3.3. Mrk 335

This object is a strong UV and X-ray source (Boller et al. 1996; Crenshaw et al. 1999; Comastri et al. 2001; Ballantyne et al. 2001). The near-IR spectrum is dominated by He I λ10830 and the H I Paschen lines (Fig. 3). The 1 μm Fe II feature is not as strong as in the former two galaxies. In addition, Fe II λ11127 and Paα are affected by atmospheric absorption. The Ca II triplet in emission, although present, is weak. The λ9220 feature is rather strong. From the Gaussian fitting, we identified Fe II λ9177, λ9202, λ9256, and Pa9 as individual components of this blend. The continuum emission of this galaxy is particularly interesting: there is a broad minimum around 1.4 μm and a rapid rise toward longer wavelengths. It probably represents the shift from a nonthermal continuum to the thermal dust emission regime. In their near-IR spectrophotometry of Mrk 335, Rudy et al. (1982) pointed out that the colors of this object are among the reddest and most nonstellar reported for any Seyfert galaxy. They also conclude that the small flux at 10 and 20 μm indicates that Mrk 335 does not contain large amounts of cool dust and that the bulk of near-IR luminosity is produced by a relatively small amount of warm dust.

2.3.4. Mrk 1044

The dominant feature in the spectrum of this galaxy is He I λ10830 (Fig. 4). The 1 μm Fe II lines are present, but only λ9997 and λ10501 are easily identified. Fe II λ11127 is severely affected by atmospheric absorption, so it is only possible to derive a lower limit for the flux of this line. O I λ8446, λ11287, Ca II λ8498, λ8542, λ8662, and the λ9220 feature are other important signatures of the BLR visible in this spectrum. The NLR contribution, as in Mrk 335, is rather weak, with only [S III] λ9531 clearly observed. The continuum emission also shows a broad minimum around 1.4 μm. It is very steep blueward and mostly flat redward of 1.4 μm.

3. DISCUSSION

The spectra presented here not only confirm the presence of the 1 μm Fe II lines in NLS1s, but they are also the strongest and most prominent Fe II lines observed in the 0.8–2.4 μm interval. This suggests that the 1 μm Fe II lines are a common feature in these objects, similar to the Fe II bumps at both sides of Hβ in the optical region. In addition, fainter Fe II lines are clearly detected in the 8700–9300 Å interval. Our goal is to discuss the dominant excitation mechanism for these lines and to confirm if, as in I Zw 1, collisional excitation is the most plausible one. For this purpose, our data as well as information from other wavebands will be used. It is also important to determine if the relative intensities of the 1 μm Fe II lines vary from object to object or if, as in the optical region, they are approximately constant.

3.1. Excitation Mechanisms of the Near-IR Fe II Lines

Excitation mechanisms invoked for the Fe II emission include continuum fluorescence via the UV resonance lines, self-fluorescence via overlapping Fe II transitions, and collisional excitation. The latter two are thought to contribute to the bulk of the Fe II emission (Wills et al. 1985). Nonetheless, most models that take into account these processes fail at reproducing the observed intensity of UV and optical Fe II lines.

3.1.1. What We Have Learned from Stars

Based on the observation of Fe II lines in low-resolution *IUE* spectra of cool giants and supergiants, Johansson (1983) and Johansson & Jordan (1984) proposed a large set of pumping channels for Lyα to excite Fe II levels with excitation energy around 10 eV ($5p$ levels). The decay route from these levels include e^4D and e^6D of $3d^6(^5D)5s$, which lie at wavelengths $\sim$8000–9600 Å. These two levels decay giving rise to multiplets such as UV 399, 391, 380 ($\sim$2850 Å), 373 ($\sim$2770 Å), and 363 ($\sim$2530 Å), which supply approximately 20% of the total energy in Fe II lines between 2000 and 3000 Å (Penston 1987). In addition, Johansson & Jordan (1984) proposed Lyα fluorescence to pump a further $^4G^0$ level at $\sim$13 eV, whose primary decay to b^4G produces the UV lines at 1841, 1845, 1870, and 1873 Å.[4] A subsequent cascade to z^4F^0 would produce the 1 μm Fe II lines, as is illustrated in Figure 6.

Near-infrared spectroscopy of young stellar objects (Hamann & Simon 1988; Hamann & Persson 1989; Hamann et al. 1994; Kelly, Rieke, & Campbell 1994) has, in fact, shown most of the near-IR Fe II emission features associated with Lα fluorescence. The flux ratios measured from our objects agree with this scenario.

3.1.2. Is Lyα Fluorescence also at Work in AGNs?

In AGNs a definitive test to confirm the presence of the Lyα pumping has been elusive because of both the blending of the broad lines and the lack of suitable data in the near-IR region. Recently, Sigut & Pradhan (1998), using theoretical Fe II emission-line strengths, derived by considering all of the above four mechanisms, demonstrated that a key feature associated with Lyα pumping is signifi-

---

[4] In Johansson & Jordan (1984), the primary decay from $^4G^0$ to b^4G produces only Fe II $\lambda\lambda$1870, 1873. Nonetheless, data from the iron project also predict lines at 1841 and 1845 Å because of the fine structure of that upper level (Nahar 1995; A. K. Pradhan 2001, private communication). The current notation for $^4G^0$ is $(u, t)^4G^0$.
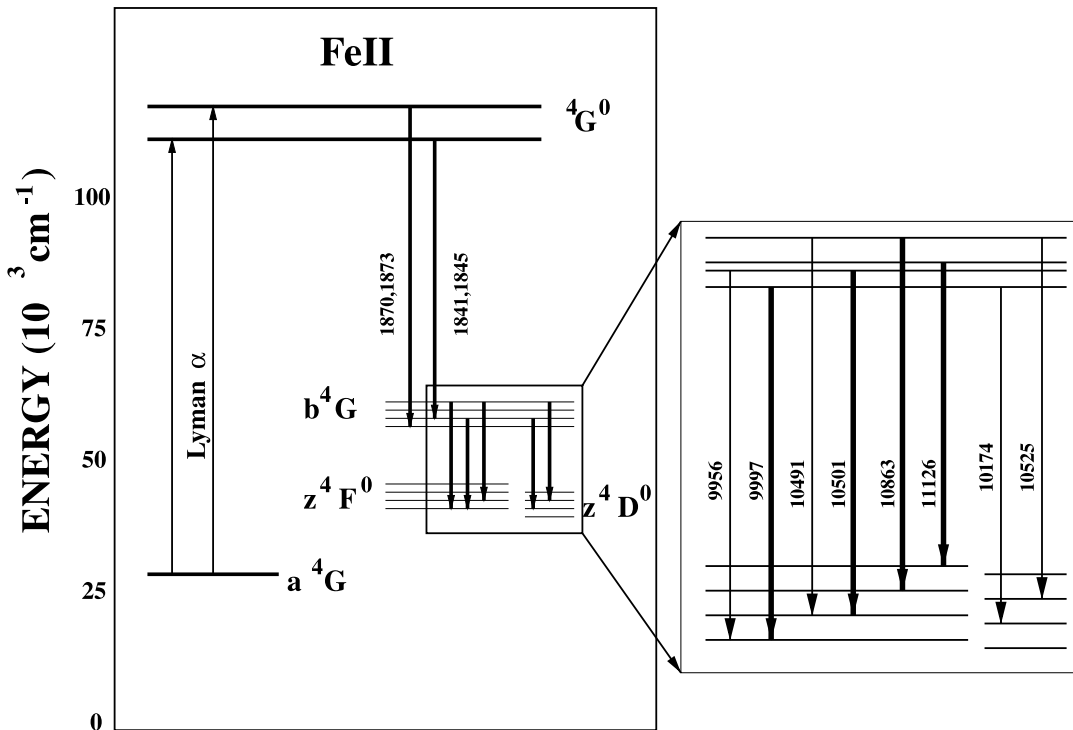
FIG. 6.—Energy level diagram for Fe II illustrating the transitions to z^4F^0 and z^4D^0 from the upper b^4G level leading to the 1 μm lines. The strongest lines observed are in bold. The excitation via Lyα fluorescence is also shown.

cant Fe II emission in the 8500–9500 Å wavelength interval. In particular, their models predict strong Fe II lines at 8490, 8927, 9130, 9177, and 9203 Å. Figure 7 shows an enlarged portion of the 8900–9300 Å region for each of the objects' spectra, clearly displaying the latter three Fe II lines and a blip at the expected position of Fe II λ8927. This result offers the first direct evidence of Lyα pumping in AGNs and will be discussed in detail in A. Rodríguez-Ardila et al. (2002b, in preparation).

If Lyα fluorescence is also responsible for the production of the 1 μm lines, the feed lines λ1841, λ1845, λ1870, and λ1873 should be observed (see Fig. 6). We have searched the *IUE* and *Hubble Space Telescope* (*HST*) Faint Object Spectrograph (FOS) public spectra available for the objects studied here to look for emission lines at these four positions. No significant emission was found, as is illustrated in Figure 8, where the region around 1860 Å in Ark 564 and Mrk 335 is shown. The spikes detected at the expected positions are almost at the noise level. Assuming that they actually correspond to $\lambda\lambda$1840, 1844 and $\lambda\lambda$1870, 1873, Table 4 gives the flux upper limit measured for these features (col. [2]) and the strength that they should need to have (assuming zero internal reddening) in order to produced the observed 1 μm lines (col. [3]). The expected values were derived assuming a one-to-one relation between the number of photons of the 1 μm and UV Fe II lines. Column (4) of that same table lists the $E(B-V)$ necessary to reduce the expected UV flux to the observed value. It was derived using the Galactic extinction law of Cardelli, Clayton, & Mathis (1989). Since that amount of reddening should conceal other UV features that are otherwise prominent, we discard this effect for explaining the weakness of the feed UV lines. Another argument against strong

reddening is the presence of a steep blue continuum in most of these objects.

There is still the possibility that these lines are, in fact, emitted but then efficiently destroyed within the BLR, but following the same line of reasoning as RMPH, other UV features should also be affected by such a destruction mechanism. Since Lyα, He II λ1640, and other important UV lines are clearly visible, we ruled out that hypothesis.

We conclude that Lyα fluorescence cannot be the only process responsible for the emission of the 1 μm Fe II lines. From the observed strength of the UV lines, that mechanism appears to have a minimal contribution to the near-IR features.

3.1.3. *Alternative Mechanisms*

An alternative process to the production of the near-IR Fe II emission is recombination. However, in addition to the 1 μm lines, a myriad of other transitions should also be

TABLE 4

MEASURED AND EXPECTED FLUX FOR THE
Fe II LINES $\lambda\lambda$1840, 1844

Galaxy (1)	Observed[a] (2)	Expected (3)	$E(B-V)$ (4)
1H1934−063	13.2	158.0	0.61
Ark 564	0.7	58.0	1.10
Mrk 335	1.7	74.9	0.93
Mrk 1044	0.6	57.0	1.12

NOTE.—Fluxes are In units of 10^{-14} ergs cm^{-2} s^{-1}. The values of columns (2) and (3) correspond to the sum of the flux of the individual Fe II features.
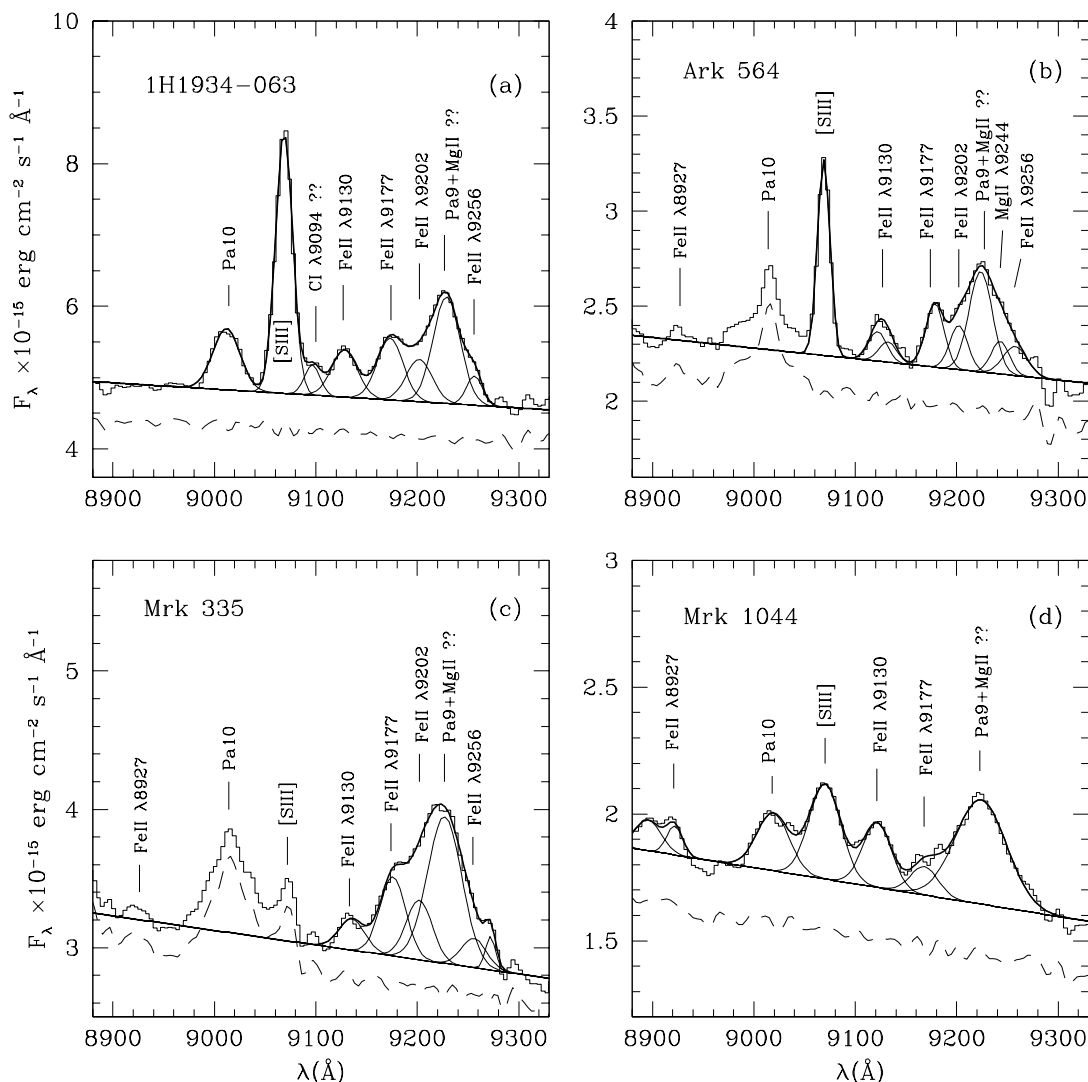
[a] Upper limit.

Fig. 7.—Zoom around the 8900–9300 Å region showing the presence of the Fe II lines at 8927, 9130, 9177, and 9202 Å. These lines are all primary cascades from Lα pumped levels at ~10 eV.

present in the 0.8–2.4 μm interval, some of them as strong or stronger than the ones around 1 μm (Kurucz 1981). Their absence clearly rules out this hypothesis.

Continuum fluorescence, first suggested by Wampler & Oke (1967), has been a popular explanation for the presence of strong Fe II emission in Seyfert 1 galaxies and quasars. In this process, the 5 eV levels of Fe II are excited by absorption of ultraviolet continuum photons in the resonance line transitions. Nonetheless, this process very unlikely contributes to populate the upper b^4G level because no resonant transitions connecting this level to the ground levels have yet been identified.

There are two other possible excitation mechanisms. The first one takes advantage of the fact that the 1 μm lines are, by far, the strongest Fe II lines observed in the 0.8–2.4 μm interval. Since they all descend from a common upper level (b^4G; see Fig. 6), their presence suggests that some sort of selective mechanism is operating to populate that particular level. Collisional pumping from the metastable a^4G level is, at least qualitatively, a viable process to explain the strength of these features in AGNs. The small energy separation between the two levels involved (~3.57 eV), the

high density of the BLR gas ($N_e \leq 10^9$ cm^{-3}), and the temperature predicted for the Fe II region by most models (~8000 K) favor this mechanism. In order to be efficient, the population of the level a^4G must be significant, i.e., above the Boltzman population. This can be done by the decay to a^4G from another set of levels such as $^4F^0$. A signature of this process is Fe II emission in the 1535–1550 Å interval. The Fe II line at 1534 Å ($5p^4F^0$–$a\ ^4G$) is a particular example of this decay route. Unfortunately, its proximity to the strong C IV λ1548 feature may hamper the detection of that emission. The a^4G levels can also be populated by decays from y^4H^0. This route produces lines in the 2430–2460 Å wavelength interval. It is also possible that b^4G is collisionally populated from the lower z^4F^0. That requires high optical depths in the strong optical and UV-permitted transitions originating from this latter level in order to keep it significantly populated. This condition seems plausible because most optical and UV Fe II multiplets are rather strong in AGNs.

The last possible process is to populate b^4G directly by decays from other levels previously pumped by Lyα fluorescence. In particular, the upper $^4F^0$ level, after absorption of
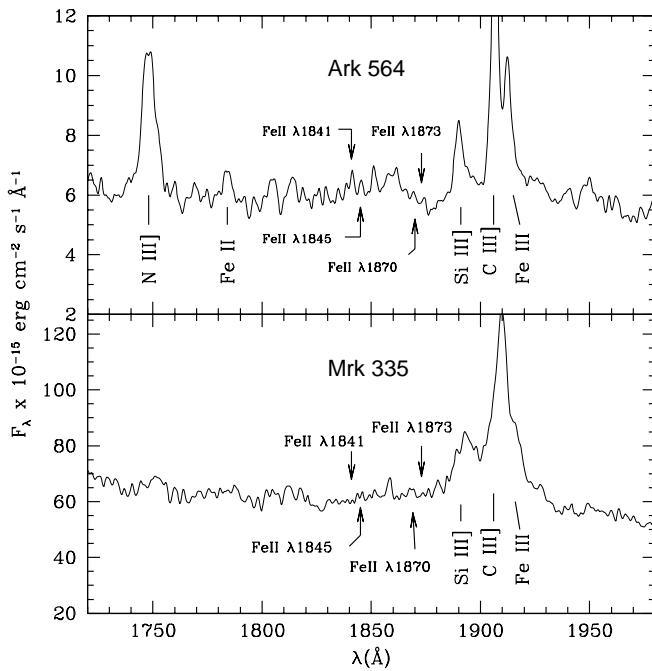
FIG. 8.—*HST*/FOS UV spectra for Ark 564 (*top*) and Mrk 335 (*bottom*) in the region around 1870 Å. The arrows mark the expected position of the Fe II lines $\lambda1841$, $\lambda1845$, $\lambda1870$, and $\lambda1873$, resulting from the primary decay of the upper u^4G^0 and t^4G^0 terms, pumped Lyα fluorescence. The presence of these lines is crucial for determining if this mechanism contributes to the production of the 1 μm Fe II lines.

an Lyα photon, may cascade directly to b^4G, emitting Fe II lines in the 2700–2770 Å interval (Fe II $\lambda2707$, $\lambda2739$, $\lambda2765$, and $\lambda2769$). In this case, no collisional excitation of b^4G is required. An inspection of the *IUE/HST* spectra of Ark 564, Mrk 335, and Mrk 1044 shows evidence of the above lines at the expected position, suggesting that this process may also contribute to the 1 μm Fe II line intensities.

3.1.4. Conclusions

In summary, clear evidence of Lyα pumping of Fe II is found from the observation of the primary cascade lines in the 8900–9300 Å interval, formed by the decay of the upper $5p$ levels to the e^4D and e^6D levels. This result confirms that fluorescence excitation by Lyα has an active role in the Fe II spectra of AGNs. Nonetheless, contrary to what was previously suggested, this same process seems to be insufficient

to explain the strength of the 1 μm lines, the strongest of all Fe II lines in the 8000–24000 Å region. This conclusion is drawn from the weakness of the primary cascade lines that feed the upper term from which the 1 μm Fe II emission originates. Our observations point to a combination of collisional excitation and decays from levels populated by Lyα photons to produce the Fe II spectrum in the near-IR.

3.2. Relative Intensities of the 1 μm Fe II Lines

One advantage of the 1 μm Fe II lines over the corresponding emission in the optical region is that most of the individual lines are clearly separated in wavelength, allowing their measurement without the need of constructing an Fe II template to quantify them. Although in most cases emission from H I, He I, and He II is near the Fe II lines, it is still possible to measure, at a good confidence level, the flux of the individual components.

In all cases our spectra show that $\lambda9997$ is the strongest Fe II transition in the near-IR. The relative fluxes of other Fe II lines compared to that of $\lambda9997$ are listed in Table 5. We have also included, for comparison, data taken from RMPH for I Zw 1 (col. [6]), Rudy et al. (1991) for LkHα 101 (col. [7]), and Kelly et al. l (1994) for MWC 249 and R Mon (cols. [8] and [9], respectively). The last three objects are Galactic sources, well known for their strong Fe II emission lines in the near-IR, which are believed to arise in a gas with physical conditions similar to those found in AGNs.

The 1 μm Fe II ratios vary from object to object, as is seen in Table 5. Comparing the values derived for our sample with those of I Zw 1 (considered as the prototype NLS1), we found that, within errors, 1H1934−063 is the most I Zw 1–like. On the other hand, Mrk 1044 deviates most significantly in regard to the Fe II emission. The situation is also highly discrepant when we compare the NLS1 ratios to those of Galactic objects. No agreement between these two groups can be seen. The ratios among the Galactic sources look rather constant, in contrast to the large scatter showed by the NLS1 data. Rudy et al. (1991) had already noted the similarity of line ratios between Lk Hα 101 and η Car, another Galactic source, and argued that this may suggest that the same process gives rise to the lines in both. They proposed Lyα fluorescence as the dominant mechanism for the production of Fe II but did not discard collisional excitation.

It may be argued that the large scatter in Fe II line ratios is due to reddening since none of the NLS1 spectra have

TABLE 5

Fe II LINE RATIOS FOR THE OBSERVED SAMPLE

Ratio (1)	1H1934−063 (2)	Ark 564 (3)	Mrk 335 (4)	Mrk 1044 (5)	I Zw 1[a] (6)	Lk Hα 101[b] (7)	MWC 349[c] (8)	R Mon[c] (9)
$\lambda9997/\lambda10171$	5.32 ± 1.78	4.53 ± 0.85	5.66 ± 0.90	6.18 ± 2.00	...	3.70	3.5	...
$\lambda9997/\lambda10501$	1.72 ± 0.20	1.32 ± 0.11	2.38 ± 0.31	1.17 ± 0.29	2.22 ± 0.29	1.11	1.6	1.5
$\lambda9997/\lambda10863$	1.07 ± 0.10	1.74 ± 0.16	...	1.04 ± 0.15	0.90 ± 0.15	1.26	...	0.98
$\lambda9997/\lambda11127$	3.47 ± 0.65	3.19 ± 0.43	7.92 ± 1.05	2.51	4.59 ± 0.76	1.59	2.00	1.9
$\lambda11127/\lambda10863$	0.31 ± 0.06	0.55 ± 0.08	...	...	0.20 ± 0.04	0.80	...	0.55
$\lambda10501/\lambda10863$	0.62 ± 0.07	1.31 ± 0.14	...	0.89 ± 0.24	0.41 ± 0.07	1.14	...	0.70
$\lambda10501/\lambda11127$	2.02 ± 0.41	2.40 ± 0.35	3.33 ± 0.94	2.23	2.06 ± 0.37	1.43	1.20	1.3
Fe II $\lambda4750$/Hβ......	0.89[d]	0.81[e]	0.47[e]	0.91[e]	1.34[e]	...	...	...

[a] Rudy et al. 2000.
[b] Rudy et al. 1991.
[c] Kelly et al. 1994.
[d] Rodríguez-Ardila et al. 2000b.
[e] Joly 1991.

been corrected for internal extinction (the Galactic source line ratios all have been corrected). However, the near-IR region is less affected by reddening than the UV and optical regions, and the wavelength interval where the 1 μm Fe II features are located is relatively small. Thus, one would expect that the reddening is not important here. In addition, all the objects have strong emission lines in the UV, indicating that the reddening is small. In order to completely avoid any reddening effect, we have calculated line ratios that are very close in wavelength and therefore insensitive to reddening. Such is the case for Fe II $\lambda 9997/\lambda 10171$, Fe II $\lambda 11127/\lambda 10863$, and Fe II $\lambda 10501/\lambda 10863$. The results, also listed in Table 5, follow the same trend in the sense that the line ratios vary from galaxy to galaxy and also differ from the line ratios derived for the Galactic sources. This variation is more clearly seen in Figure 9, where the line ratios are plotted for the objects listed in Table 5. The large scatter of the NLS1 data and the constancy among Galactic sources is evident.

The above results strongly contrast to what is observed in the optical region, where the relative intensities of the Fe II lines in AGNs seem rather similar from object to object.

Apparently, aside from the scale factor the only difference between the optical Fe II features of two given objects is the width of the individual lines. This result was clearly illustrated in Phillips (1978) by comparing the Fe II emission in the 4400–5300 Å region of several Seyfert 1 galaxies. The Fe II emission in that same interval for I Zw 1, Ark 564, and 1H1934$-$063 is shown in Figure 10. Note how similar the Fe II multiplets in these objects are. For that reason, usually I Zw 1, which has one of the narrowest permitted lines in Seyfert 1 galaxies, is used as a template to determine the strength of the Fe II emission (Boroson & Green 1992; Rodríguez-Ardila, Pastoriza, & Donzelli 2000b).

The question that arises now is if there is a correlation between the strength of the Fe II in the optical and near-IR. Figure 11 shows Fe II/Hβ versus Fe II IR/Pa δ. The former is the flux of the Fe II emission centered at 4570 Å, which scales with the total optical Fe II, normalized to Hβ, while the latter is the sum of the Fe II lines $\lambda 9997$, $\lambda 10171$, and $\lambda 10501$ normalized to the Paδ flux. Except for Mrk 335 (the galaxy with the smallest Fe II/Hβ), Fe II $\lambda 9997$ seems to scale with the corresponding optical Fe II. That correlation is very important since most of the optical Fe II lines in the
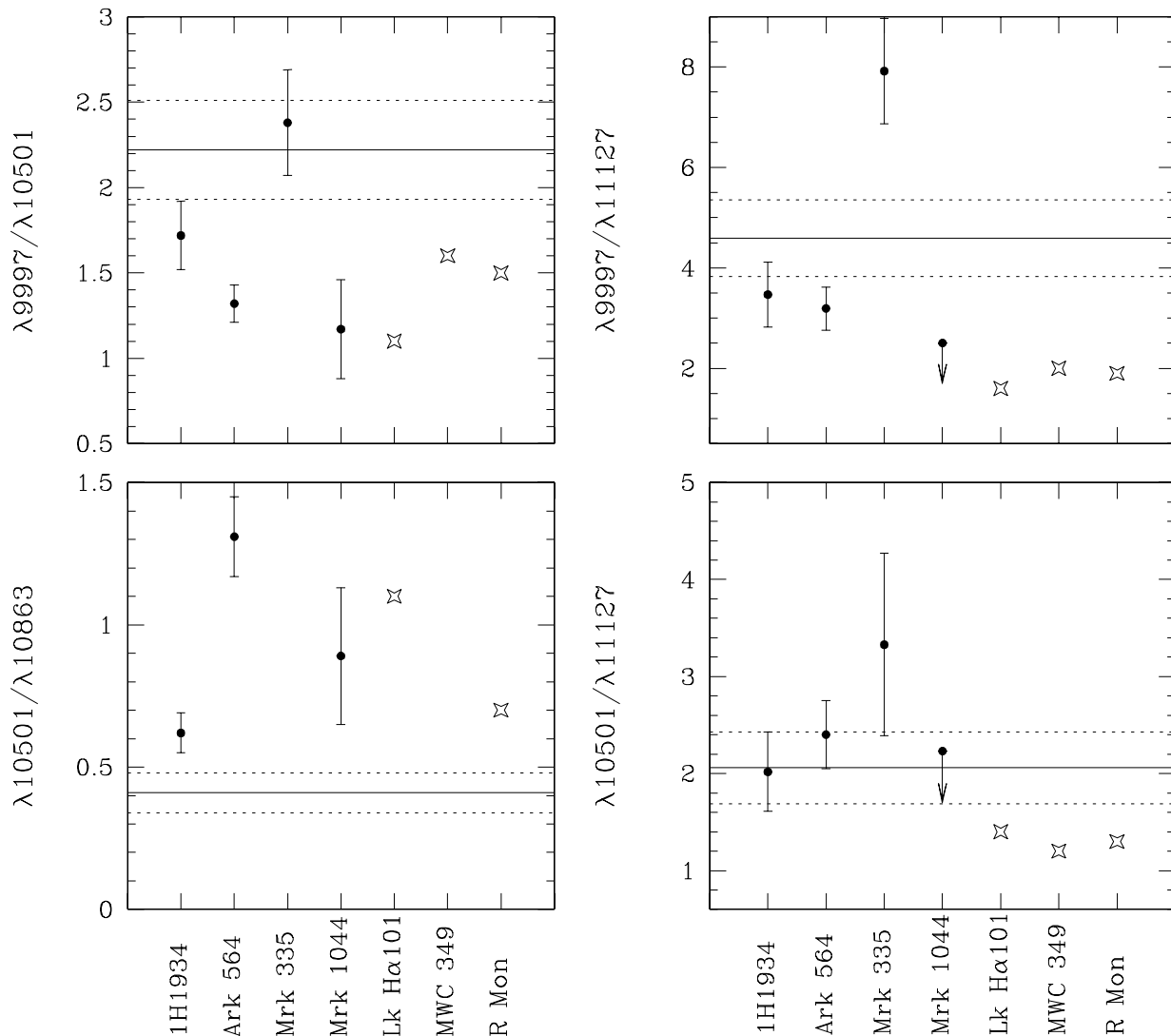

Fig. 9.—Ratios between the most important Fe II lines observed in the galaxies and the Galactic sources Lk Hα101, MWC 349, and R Mon. The solid line is the value reported by RMPH for I Zw 1, and the dotted line corresponds to the uncertainty. The stars correspond to the Galactic sources.
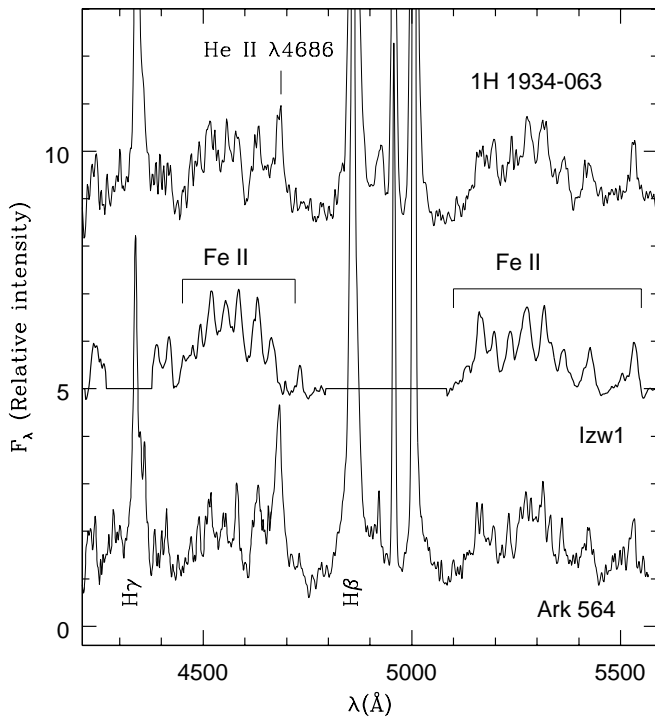
FIG. 10.—Comparison of the optical Fe II spectra of 1H1934−063 (*top*), I Zw 1 (*middle*), and Ark 564 (*bottom*). Except for the width of the individual lines (narrower in Ark 564), the three spectra look similar. Note that the relative intensities of the Fe II lines seem to be constant in the three objects. The Hβ and Hγ lines of I Zw 1 were removed for clarity.

wavelength interval 4400–5300 Å arise from the same upper two upper levels z^4F^0 and z^4D^0. Although no definitive conclusions can be drawn because of the reduced number of points, Figure 11 clearly suggests that the optical Fe II emission is directly linked to the 1 μm Fe II lines. In this sce-
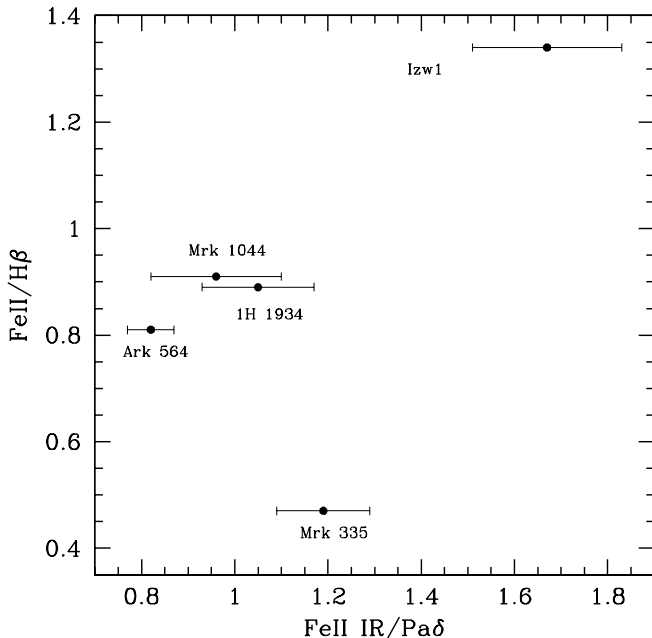
FIG. 11.—Optical Fe II emission (Fe II $\lambda4750$/Hβ) vs. the sum of the flux of Fe II $\lambda9997$, $\lambda10171$, and $\lambda10501$ divided by Paδ (Fe II IR/Paδ). Values of Fe II $\lambda4750$/Hβ are listed in Table 5. Mrk 335 clearly departs from an apparent correlation between these two quantities.

nario, decay from b^4G^0 largely contributes to the population of those two levels. Although a detailed balance between the energy carried by the near-IR and optical Fe II lines is far from the scope of this paper, this result is important for current Fe II modeling.

Factors such as different optical depth effects and, possibly, different sensitivities to physical parameters between the near-IR and optical Fe II lines can be invoked to explain why the line ratios in the former region present more scatter than those of the latter. Additional observations in a larger sample of objects and a more accurate modeling of the 1 μm Fe II lines are needed to explain this trend. It is also interesting to understand why Mrk 335 deviates so much from the other NLS1s. While its optical Fe II is rather low for a typical NLS1, its near-IR Fe II ranks it as a strong emitter.

4. KINEMATICS OF THE BLR

The quality and spectral resolution of the SPEX data allow us to study and compare, for the first time, the form and width of the different near-IR permitted emission-line profiles of AGNs and, in particular, of NLS1s. This is important for at least two reasons. First, it has been argued (from both theoretical models and observational grounds) that low-ionization lines such as Fe II, O I, Mg II, Ca II, and Balmer lines are formed in a distinct, separate zone (most probably the outer part of the BLR) from the place where most high-ionization lines (i.e., Lyα, He II, and Ca IV) are produced (Collin-Souffrin et al. 1986; Rodríguez-Pascual, Mass-Hesse, & Santos-Llèo 1997). Differences in line widths between low- and high-ionization lines are usually interpreted as evidence of this stratification, provided that the velocity field does not differ strongly from gravitationally bound Keplerian or virial motion, as seems to be the case for most AGNs (Peterson & Wandel 1999). Second, the presence of asymmetries in the line profiles helps to distinguish between radial and rotational motions, setting constraints on the velocity field of the BLR.

Although the visible and UV spectral regions in AGNs are full of permitted emission lines, usually they are severely blended, affecting the placement of the continuum level and the separation of the individual profiles. Such is the case with the Fe II lines, which form a pseudocontinuum even in NLS1s because of their close proximity. The near-IR region is promising in this respect (if the resolution is high enough). Lines such as Ca II $\lambda8664$, Fe II $\lambda11127$, O I $\lambda11287$, and Paβ are completely isolated or mildly blended, making their separation and the analysis of their emission profiles easier.

For the above reasons, we have chosen Fe II $\lambda11127$, O I $\lambda11287$, O I $\lambda8446$, and Ca II $\lambda8664$ as representative of low-ionization BLR lines and Paβ as an example of a BLR recombination line. By comparing their emission-line profiles, we expect to get clues about the structure and kinematics of the emitting region. In addition, we have used the [S III] $\lambda9531$ profile to represent the velocity field of the NLR.

The observed profiles of Paβ, Fe II $\lambda11127$, O I $\lambda11286$, and [S III] $\lambda9531$ are shown in velocity space in Figure 12. In order to easily compare them, the peak intensity of each line has been normalized to unity. In all cases, Paβ has been stripped of the narrow component by subtracting the contribution from the NLR according to the procedure explained in § 2. Since the Fe II and the O I emission are features restricted to the BLR, there is no need to determine such a contribution in these two lines.
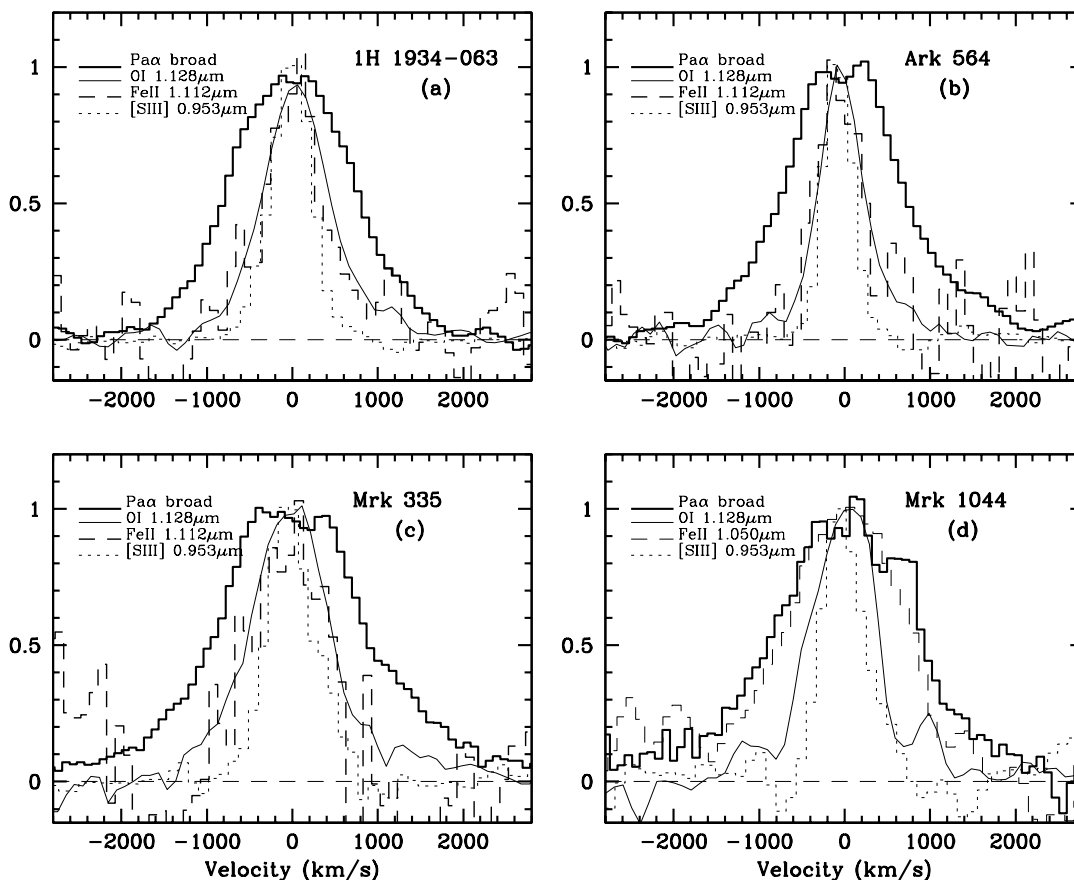
FIG. 12.—Comparison of the line profiles of Paβ (*thick histogram*), O I λ11287 (*solid line*), Fe II λ11127 (*dashed histogram*), and [S III] λ9531 (*dotted histogram*) in velocity space, showing clearly that Paβ is significantly wider than the lines emitted in the partially ionized zone of the BLR. This suggests that low-ionization lines such as Fe II and O I form in the outermost part of the BLR.

The results are surprising. Except for Mrk 1044, Fe II and O I share almost the same velocity field and display very similar line profiles. However, they are significantly narrower than Paβ. In fact, they are just slightly broader than [S III] λ9531. Assuming that this latter line is formed in the inner portion of the NLR (its critical density N_c is $\sim 10^{7.5}$ cm^{-3}), the small width of Fe II and O I indicates that we are probably looking at the outer boundaries of the BLR. The result obtained for Mrk 1044 can be explained if we recall that in Figure 12 the Fe II profile plotted corresponds to that of λ10501 instead of λ11127 because this latter line is severely affected by atmospheric absorption (see § 2.3.4). Fe II λ10501 is, in fact, a blend of two Fe II lines located at 10491 and 10501 Å. Observations in stars (Rudy et al. 1991) show that the latter line is about 5 times stronger than the former (in which case the effect of λ10491 on the blend width would be negligible). A lower ratio may cause λ10501 to appear broader, as seems to be the case for Mrk 1044 as well as for Ark 564 (see Table 2).

Assuming that the clouds emitting the broad lines are gravitationally bound to the central mass concentration and that the velocity field is Keplerian, Figure 12 clearly supports the hypothesis that Fe II and O I are emitted in the outer part of the BLR, while most of the Paβ flux is formed in the intermediate portion of this region. This result is compatible with the physical conditions needed to form permitted Fe II and O I, i.e., neutral gas strongly shielded from the incident ionizing radiation of the central source,

conditions which can only be met deeper within the neutral zone of the outermost part of the BLR.

The above results seem to contradict those of Morris & Ward (1989), who compared the Hα and O I λ8446 line profiles in a sample of 12 objects. They found no evidence for differences between the profiles of these two lines. Nonetheless, recall that Paβ is less affected than Hα by radiation transport effects. When crossing the BLR, Hα photons produced in inner higher velocity clouds are more likely to be absorbed than Paβ photons. Thus, the Hα line probes the outer low-velocity clouds, while the Paβ profile shows the contribution from inner high-velocity clouds. For the above reason, we expect Paα to be broader than Hα as well as broader than low-ionization lines such as O I and Fe II. The most important point here is that Figure 12 shows that low-ionization BLR lines are emitted almost at the border between the BLR and NLR.

Another interesting result that can be drawn from Figure 12 is the difference in the form of the profiles from object to object: in 1H1934−063 they are typically Gaussian, while in Ark 564 they are mostly Lorentzian, with Mrk 335 and Mrk 1044 being intermediate cases. This is valid not only for Paα but also for Fe II and O I. Since the spectra were taken at the same resolution with the same telescope and setup, this clearly indicates differences in the velocity fields of the objects.

It is also possible to probe weakly ionized material within the BLR by means of Ca II λ8664, one of the Ca near-IR

triplet lines that is perfectly isolated and has good S/N in our data. The observed Ca II $\lambda8664$ is compared to that of O I $\lambda8446$ in Figure 13. Clearly, these two lines have very similar form and width, indicating that they share the overall kinematics of the region where they are emitted. This was already pointed out by Persson (1988) in his study of the Ca II and O I lines in 14 of 40 AGNs for which simultaneous emission of these two ions was found. Here, our results not only agree with those of Persson (1988) but also extend that analysis to Fe II and show that those three lines should have similar kinematics. Because of the high complexity the Fe II atom, its spectrum is far from being understood. Information derived for O I or Ca II (i.e., column density and ionization parameters) provides valuable constraints for modeling the Fe II atom given that these species seem to form from the same ensemble of clouds.

The importance of the Ca II emission as a valuable diagnostic of the BLR is stressed by Ferland & Persson (1989). Using photoionization models that reproduce well both the high- and low-ionization line intensities, they found that clouds with extremely high column densities ($N_H \sim 10^{25}$

cm^{-2}) are needed to emit Ca II. The large N_H suggests that the clouds might be a wind or corona above a star or accretion disk. It is well known that a wind scenario usually produces asymmetries in the observed profiles. The Ca II line profiles in Ark 564 marginally show evidence of asymmetries toward the blue (upper right-hand panel of Fig. 13). High-resolution spectroscopy around this region is highly desirable to find additional clues about the kinematics of the outer portion of the BLR. Our results stress the kinematic connection between the low-ionization species and confirm previous claims that the understanding of the mechanisms leading to the formation of the Fe II and Ca II lines is crucial for solving the puzzle associated with the geometry and physical conditions of the outer parts of the BLR.

In summary, the comparison of the near-IR broad emission-line profiles definitively shows the presence of a stratification within the BLR. Low-ionization lines such as Fe II, O I, and Ca II are emitted in the outer edge of the BLR. Paβ emission, on the other hand, maps the velocity field of the inner portions of the BLR.
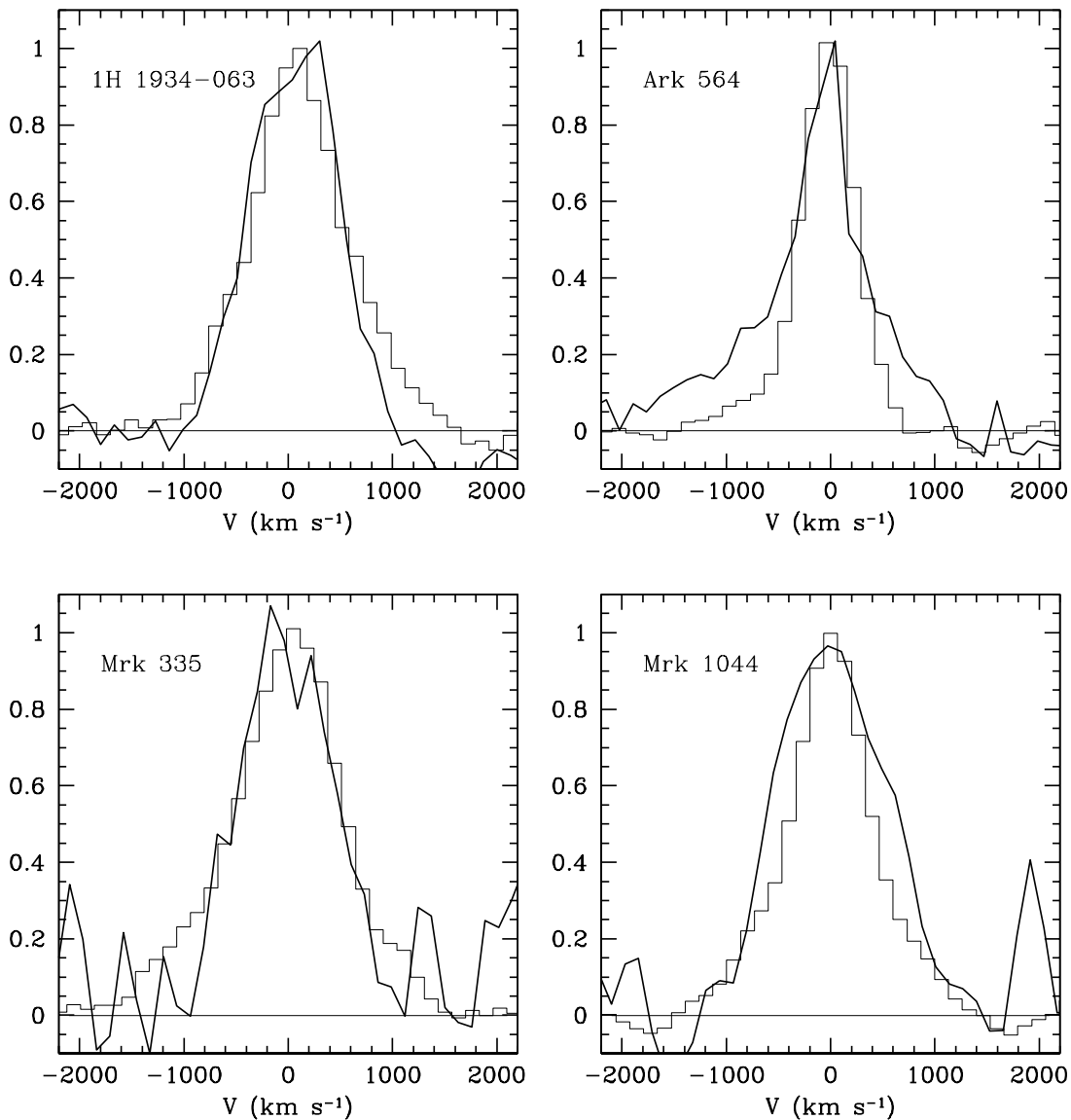

FIG. 13.—Comparison of the emission-line profiles of Ca II $\lambda8662$ (*thick line*) and O I $\lambda8446$ (*histogram*) in velocity space

5. CONCLUSIONS

We have analyzed four NLS1 spectra in the 0.8–2.4 μm wavelength range in order to study the Fe II emission and the kinematics of the BLR. The results show that the Fe II emission in the 8500–9300 Å interval and around 1 μm is a common feature of this class of AGNs. The Fe II lines in the former interval are, for the first time, resolved in this type of object. Since they are primary cascades of the upper $5p$ levels pumped by Lyα fluorescence, our data offer clear observational evidence for the presence of this excitation mechanism in AGNs. The Fe II lines located at 9997, 10501, 10863, and 11127 Å, which share the same upper and lower levels (b^4G and z^4F^0, respectively), are very prominent and are the strongest Fe II lines in the four spectra. Although Lyα fluorescence indirectly contributes to their production, that mechanism cannot explain their full strength because of the weakness of the UV Fe II lines that feed the upper b^4G level. Collisional ionization, mainly from the a^4G and z^4F^0 levels, is suggested as an additional mechanism that plays an active role in exciting the 1 μm Fe II lines.

The near-IR Fe II line ratios (i.e., $\lambda 9997/\lambda 10501$ and $\lambda 10501/\lambda 10863$) show a large scatter from object to object, contrary to what is observed in the optical region. Nonetheless, the apparent good correlation found between the Fe II emission of these two wavelength intervals supports a common origin. Since most of the optical Fe II multiplets originate in transitions from z^4F^0, that level would be mainly populated by the decay from b^4G.

The emission-line profiles of Fe II, O I, and Ca II are very similar in form and width but significantly narrower than that of Paβ. This strongly suggests that the Ca II, Fe II, and O I regions are cospatial and kinematically linked. More-over, because their profiles are just slightly broader than that of [S III] $\lambda 9531$, low-ionization BLR lines are most likely formed in the outermost portion of the BLR. This is compatible with the physical conditions required to form them: cool gas with high column densities that provides a shield from the incident ultraviolet continuum of the central source and a location deep within the neutral zone of the BLR. The larger width of the Paschen lines indicates that they are suitable for mapping the gas located at interme-diate positions in the BLR.

Given the high complexity of the Fe II atom and its ubiquitous emission in AGNs, only detailed model calcu-lations that take into account all possible excitation mecha-nisms and transitions among the levels can shed some light on the dominant processes involved in the excitation of this atom. The data presented here provide valuable constraints for understanding this complex emission.

[5] Available at http://www.pa.uky.edu/~4peter/atomic.

REFERENCES

Ballantyne, D. R., Iwasawa, K., & Fabian, A. C. 2001, MNRAS, 323, 506
Boller, Th., Brandt, W. N., & Fink, H. 1996, A&A, 305, 53
Boroson, T. A., & Green, R. F. 1992, ApJS, 80, 109
Cardelli, J. A., Clayton, G. C., & Mathis, J. S. 1989, ApJ, 345, 245
Collin-Souffrin, S., Dumont, S., Joly, M., & Péquignot, D. 1986, A&A, 166, 27
Comastri, A., et al. 2001, A&A, 365, 400
Crenshaw, D. M., Kraemer, S. B., Boggess, A., Maran, S. P., Mushotzky, R. F., & Wu, C. 1999, ApJ, 516, 750
Cushing, M. C., Vacca, W. D., & Rayner, J. T. 2002, PASP, in press
Ferland, G. J., & Persson, S. E. 1989, ApJ, 347, 656
Hamann, F., DePoy, D. L., Johansson, S., & Elias, J. 1994, ApJ, 422, 626
Hamann, F., & Persson, S. E. 1989, ApJS, 71, 931
Hamann, F., & Simon, M. 1988, ApJ, 327, 876
Johansson, S. 1983, MNRAS, 205, 71P
Johansson, S., & Jordan, C. 1984, MNRAS, 210, 239
Joly, M. 1991, A&A, 242, 49
Kelly, D. M., Rieke, G. H., & Campbell, B. 1994, ApJ, 425, 231
Kurucz, R. 1981, SAO Spec. Rep. 390
Leighly, K. M. 1999, ApJS, 125, 317
Lipari, S., Terlevich, R., & Macchetto, F. 1993, ApJ, 406, 451
Morris, S. L., & Ward, M. J. 1989, ApJ, 340, 713
Nahar, S. N. 1995, A&A, 293, 967
Osterbrock, D. E., & Pogge, R. W. 1985, ApJ, 297, 166
Penston, M. V. 1987, MNRAS, 229, 1P
Persson, S. E. 1988, ApJ, 330, 751

Peterson, B., et al. 2000, ApJ, 542, 161
Peterson, B., & Wandel, A. 1999, ApJ, 521, L95
Phillips, M. M. 1978, ApJ, 226, 736
Pogge, R. W., & Owen, J. M. 1993, Ohio State Univ. Int. Rep. 93-01
Rayner, J. T., Toomey, D. W., Onaka, P. M., Denault, A. J., Stahlberger, W. E., Watanabe, D. Y., & Wang, S.-I. 1998, Proc. SPIE, 3354, 468
———. 2002, PASP, in press
Rodríguez-Ardila, A., Binette, L., Pastoriza, M. G., & Donzelli, C. J. 2000a, ApJ, 538, 581
Rodríguez-Ardila, A., Pastoriza, M. G., & Donzelli, C. J. 2000b, ApJS, 126, 63
Rodríguez-Pascual, P. M., Mass-Hesse, J. M., & Santos-Lleò, M. 1997, A&A, 327, 72
Rudy, R. J., Erwin, P., Rossano, G. S., & Puetter, R. C. 1991, ApJ, 383, 344
Rudy, R. J., Jones, B., Le Van, P. D., Puetter, R. C., Smith, H. E., Willner, S. P., & Tokunaga, A. T. 1982, ApJ, 257, 570
Rudy, R. J., Mazuk, S., Puetter, R. C., & Hamann, F. 2000, ApJ, 539, 166 (RMPH)
Schlegel, D. J., Finkbeiner, D. P., & Davis, M. 1998, ApJ, 500, 525
Sigut, T. A. A., & Pradhan, A. K. 1998, ApJ, 499, L139
Vaughan, S., Reeves, J., Warwick, R., & Edelson, R. 1999, MNRAS, 309, 113
Verner, E. M., Verner, D. A., Korista, K. T., Ferguson, J. W., Hamann, F., & Ferland, G. J. 1999, ApJS, 120, 101
Wampler, E. J., & Oke, J. B. 1967, ApJ, 148, 695
Wills, B. J., Netzer, H., & Wills, D. 1985, ApJ, 288, 94